

High Resolution Near-Infrared Spectroscopy of Cool Dwarf Stars

Andrea Dupree¹, Nancy Brickhouse¹, Jonathan Irwin¹, Robert Kurucz¹, and Elisabeth Newton²

¹ Center for Astrophysics | Harvard & Smithsonian, Cambridge, MA USA

² Massachusetts Institute of Technology, Cambridge, MA USA and Dartmouth College, Hanover, NH USA

Abstract

We present results from a near infrared survey of the He I line ($\lambda 10830\text{\AA}$) in cool dwarf stars taken with the PHOENIX spectrograph at the 4-m Mayall telescope at Kitt Peak National Observatory. Spectral synthesis of this region reproduces some but not all atomic and molecular features. The equivalent width of the He line appears directly correlated with the soft X-ray stellar surface flux except among the coolest M dwarf stars, where the helium is surprisingly weak.

1 Introduction

The near IR spectra of cool stars are little studied to date, however they contain diagnostics useful to identify warm plasma via the He I transition at $\lambda 10830\text{\AA}$ marking the presence of $\sim 15000\text{K}$ material. In addition the line profile can indicate mass motions because the transition arises from a metastable level, giving it a long lifetime to allow tracking of atmospheric dynamics. This is very pronounced in luminous cool stars (Dupree et al. 2009). Most recently, the helium line has emerged as a significant tracer of escaping exoplanet atmospheres (Oklopčić, A. & Hirata, C. M. 2018; Spake et al. 2018).

2 Near-IR Spectra of Cool Dwarfs

The PHOENIX spectrograph at the 4-m Mayall telescope at KPNO was used during February 2013 and 2014 to obtain near-IR spectra with the J9232 filter. A summary of the exposures is given in Table 1. The section near $\lambda 10830$ is shown in Fig. 1 where the stars are ordered according to their photometric colors as measured by GAIA DR2 (Evans et al. 2018).

Table 1: Phoenix Spectral Observations

Target	Date	Exposure ¹ s(repeat)
GJ 158	2456703.6218	600(2)
GJ 338A	2456704.7003	900(2)
GJ 368	2456701.0066	60(4)
GJ 380	2456703.7250	600(2)
GJ 412A	2456703.0414	900(2)
GJ 449	2456701.0131	60(4)
GJ 566A	2456702.9759	60(2)
GJ 566B	2456702.9790	90(2)
GJ 1101	2456346.6375	1500(4)
GJ1154	2456346.8192	1500(4)
NLTT 35712	2456346.9779	1500(4)

¹Exposure times are listed; in the infrared spectral region, exposures on the target are paired with a spatial offset. The number of paired exposures is shown in parentheses.

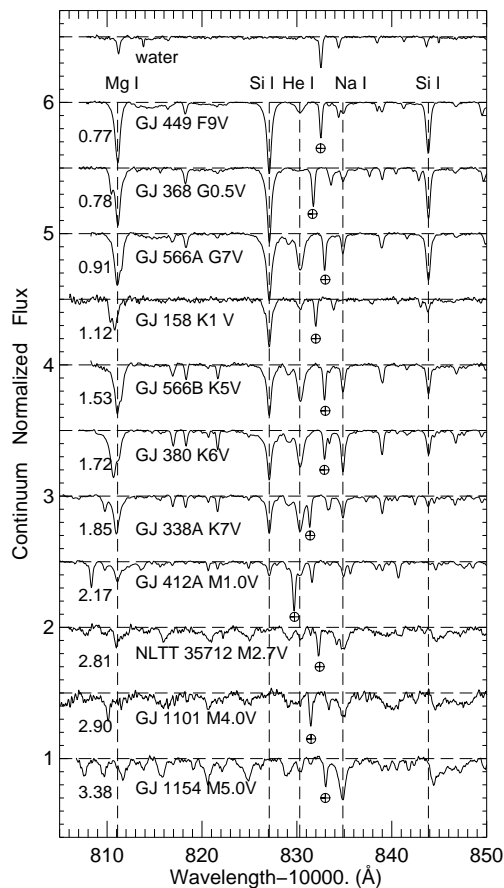


Figure 1: Near-IR spectra of cool dwarf stars. GAIA2 colors ($BP - RP$) are marked (Evans et al. 2018). Note the weakening of most atomic lines with later spectral type and the increasing strength of the Na I transition. The He I absorption exhibits varying strength discussed in Section 3.

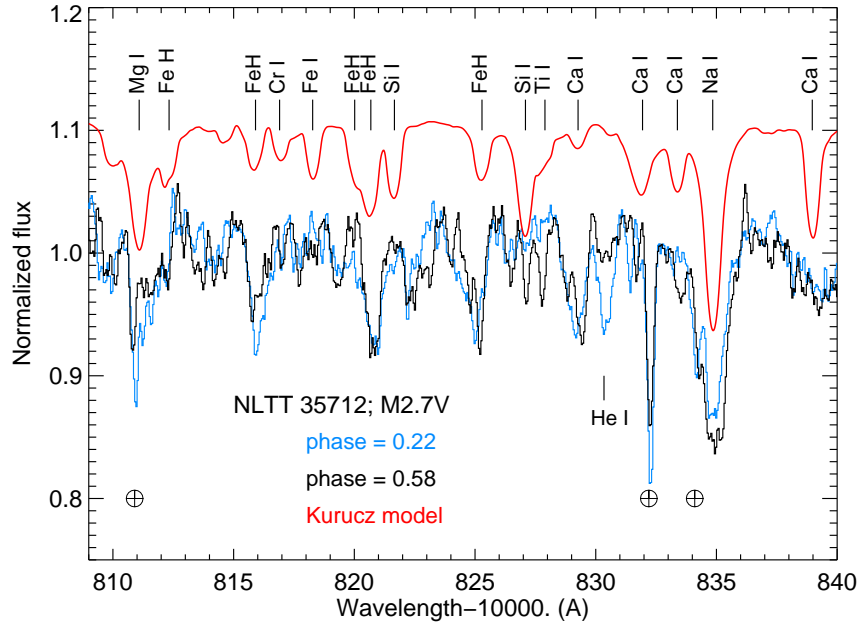


Figure 2: PHOENIX near-IR spectrum taken at the 4-m Mayall Telescope at KPNO. Spectrum calculated with a Kurucz LTE model is shown. The strong atomic features are reproduced, however several strong features remain unidentified.

The warmer objects, of spectral type F–K exhibit easily identifiable atomic transitions of neutral species (i.e. Mg I, Si I, Na I) in addition to the He I transition. These atomic species become weaker and the spectrum more complex in the cooler dwarf stars – beginning with late K spectral type and continuing into the M dwarfs. The Na I transition (10834.848Å) appears as an anomaly, becoming stronger through the spectra of the M dwarfs

To identify spectral features, an LTE photospheric model corresponding to the parameters of a \sim M2 V star was constructed (kurucz.harvard.edu) assuming $T_{eff} = 3500\text{K}$, $\log g=5$, $v_{rot}=10 \text{ km s}^{-1}$, and solar abundances. Several molecules are also included: FeH, TiH, TiO, VO, and H₂O. The synthesized spectrum is shown in Figure 2 along with observed spectra of NLTT 35712. The dominant Na I feature is reproduced in the calculation, as well as Mg I. The He I transition does not appear in the synthesized spectrum because the stellar model does not include a chromosphere. While there is good agreement in some features, many others are not identified. So there is room for improvement.

Particularly noteworthy in the spectrum of NLTT 35712 is the change in the strength of the He I line at 10830Å with stellar rotational phase. The spectra (Fig. 2) were taken at two different photometric phases of NLTT 35712: 0.22 (close to photometric minimum) and 0.58 (approaching photometric

maximum). The He I line is stronger near photometric minimum. A simple interpretation of the photometry based on solar behavior suggests that dark starspots are present near photometric minimum. If similar to the solar example, these starspots result from magnetic activity and would be associated with enhanced heating and EUV and X-ray radiation. High energy radiation can cause an increase in strength of the of the helium transition resulting from photoionization of He I and recombination into the metastable triplet level, although this effect may be mitigated when high densities are present (Sanz-Forcada and Dupree 2008).

3 Helium Line Strength Correlations

The equivalent width of the He I line is shown in Figure 3 as a function of the GAIA2 color (*left panel*) and the soft X-ray stellar surface flux (*right panel*). With the exception of the F through early K stars, the helium equivalent width decreases with later spectral type. The 3 early type stars with small equivalent widths (GJ 368, GJ 449, and GJ 158) are single (Fuhrmann et al. 2017), and in one case, metal poor (GJ 158 = HD 25329; [Fe/H]=−1.7; Gratton et al. 2000). The strength of the helium line does not depend on metallicity in dwarf stars (Takeda & Takada-Hidai 2011; Smith et al. 2012), and the upper limits are comparable among the 3 warmest stars (Pizzolato et al. 2000; Smith et al. 2016). X-ray surface fluxes, considered to be more representative of magnetic activity (Johnstone and Güdel 2017), are given in Table 2. The 3 early-type stars appear to illustrate the case where the lower

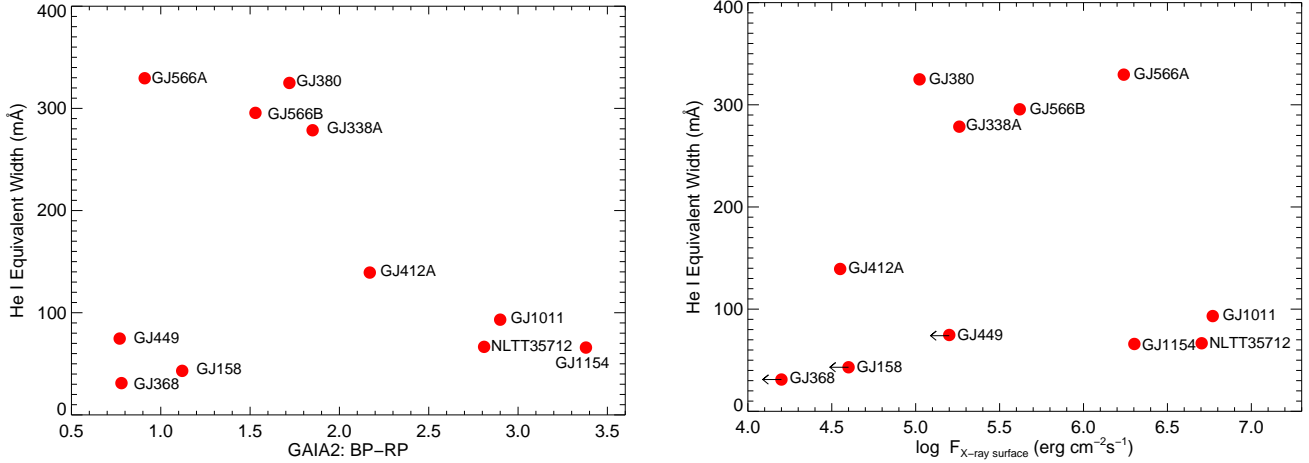


Figure 3: *Left panel*: He I equivalent width as a function of GAIA color, *Right Panel*: He I equivalent width as a function of X-ray surface flux.

level of the helium line is populated by collisions, and photoexcitation does not play a role.

At the same GAIA2 colors as the weak group, ($B - P \sim 1.5$) the stars GJ 566A and GJ 566B, although only slightly metal poor ($[\text{Fe}/\text{H}] = -0.26$, Allende Prieto et al. 2004), possess stronger X-ray surface fluxes, by a factor of 10 or more than found in GJ 367, GJ 449, and GJ 158. Also the component A (GJ 566A) with the larger helium equivalent width possesses an X-ray surface flux, larger by a factor of 4 than GJ 566B. Figure 3 suggests that the strength of the He I line is related to the surface X-ray flux for the F to early M spectral types.

However this correlation changes dramatically in the coolest objects (GJ 1011, GJ 1154, and NLTT 35712) which have the largest surface X-ray flux in the sample, yet display weak helium absorption. The cause of this change is not clear. These 3 stars have strong $H\alpha$ emission (Newton et al. 2017) indicating a chromosphere is present. These stars lie in the fully convective regime where Morin et al. (2010) suggest that radically different magnetic topologies can occur as compared to the more massive dwarf stars. The star GJ 1154 has a very strong large-scale magnetic field that is mostly poloidal and axisymmetric.

The weakness of the helium line could suggest a distinctly different atmospheric structure. Perhaps the chromosphere is substantially thinner, or smaller in surface extent in the later type M dwarfs as compared to the earlier types. Without detailed models, it is difficult to predict the structure. Inspection of the near-IR spectra in Fig. 1, shows that the coolest stars have distinctly strengthened, Na I at 10834.9Å as compared to the Si I transition at 10827Å. The Si I line arises from a 4.9eV level versus 3.6eV for the Na I transition, suggesting the increasing presence of cooler atmospheric regions.

On the other hand, studies of the near-ir helium line in metal-poor dwarf stars suggest that a span in equivalent width values of He I of a factor amounting to 2.5 to 3.5 can occur in stars with similar X-ray fluxes (Takeda & Takada-Hadai 2011). Additional stars are needed to determine the

Table 2: Target Characteristics

Target	Gaia2 color $BP-RP$	Sp. Type	He I mÅ	$\log F_X^1$	Ref.
GJ 158	1.12	K1V	43	<4.6	2,4
GJ 338A	1.85	K7V	279	5.26	2,5
GJ 368	0.78	G0.5V	31	<4.2	2,3
GJ 380	1.72	K6V	325	5.02	1,2
GJ 412A	2.17	M1.0V	139	4.55	1,2
GJ 449	0.77	F9V	75	<5.2	2,3
GJ 566A	0.91	G7V	330	6.24	2,6
GJ 566B	1.53	K5V	296	5.62	2,6
GJ 1101	2.90	M4.0V	93	6.77	1,2
GJ 1154	3.38	M5.0V	66	6.27	1,2
NLTT 35712	2.81	M2.7V	67	6.70	2,7

NOTE: ¹X-ray stellar surface flux (erg cm⁻²s⁻¹).

References: (1) Schmitt & Lfke (2004);

NeXXus2 (<http://www.hs.uni-hamburg.de/DE/For/Gal/Xgroup/nexus/index.html>)

(2) GAIA2, Evans et al. (2018) (3) Pizzolato et al. (2000)

(4) Smith et al. (2016) (5) Wood et al. (2012)

(6) Johnstone & Güdel (2015) (7) Voges et al. (1999)

extent of the variability here.

This work has made use of data from the European Space Agency (ESA) mission *Gaia* (<https://www.cosmos.esa.int/gaia>), processed by the *Gaia* Data Processing and Analysis Consortium (DPAC, <https://www.cosmos.esa.int/web/gaia/dpac/consortium>). Funding for the DPAC has been provided by national institutions, in particular the institutions participating in the *Gaia* Multilateral Agreement. This research has made use of NASA's Astrophysics Data System Bibliographic Services and the VizieR catalogue access tool, CDS, Strasbourg, France.

4 References

- Allende Prieto, C., Barklem, P. S., Lambert, D. L., & Cunha, K. 2004, *A&A*, 420, 183
- Dupree, A. K., Smith, G. H., & Strader, J. 2009, *AJ*, 138, 1485
- Evans, D. W., Riello, M., DeAngeli, F. et al. 2018, *A&A*, 616, A4
- Fuhrmann, K., Chini, R., Kaderhandt, L., and Chen. Z. 2017, *ApJ*, 836, 139
- Gratton, R. G., Sneden, C., Carretta, E., & Bragaglia, A. 2000, *A&A*, 354, 169
- Johnstone, C. P., & Güdel, M. 2015, *A&A*, 578, A129
- Morin, J., Donati, J.-F., Petit, P. et al. 2010, *MNRAS*, 407, 2269
- Newton, E. R., Irwin, J., Charbonneau, D. et al. 2017, *ApJ*, 834, 85
- Oklopčić, A. & Hirata, C. M. 2018, *ApJ*, 855, L11
- Pizzolato, N., Maggio, A., & Sciortino, S. 2000, *A&A*, 361, 614
- Sanz-Forcada, J., & Dupree, A. K. 2008, *A&A*, 488, 715
- Schmitt, J. H. M. M. & Liefke, C. 2004, *A&A*, 417, 651
- Smith, G. H., Dupree, A. K., & Günther, H. M. 2016, *AJ*, 152, 43
- Smith, G. H., Dupree, A. K., & Strader, J. 2012, *Pub. ASP*, 124, 1252
- Spake, J. J., Sing, D. K., Evans. T. M., et al. 2018, *Nature*, 557, 68
- Takeda, Y., & Takada-Hidai, M. 2011, *PASJ*, 63, S547
- Voges, W., Aschenbach, B., Boller, Th. et al. 1999, *A&A*, 349, 389
- Wood, B. E., Laming, J. M. & Karovska, M. 2012, *ApJ*, 753, 76